Defect dynamics in annealed ZnO by positron annihilation spectroscopy

Sreetama Dutta, Mahuya Chakrabarti, S. Chattopadhyay, Debnarayan Jana, D. Sanyal, and A. Sarkar

Citation: Journal of Applied Physics **98**, 053513 (2005); doi: 10.1063/1.2035308
View online: http://dx.doi.org/10.1063/1.2035308
View Table of Contents: http://scitation.aip.org/content/aip/journal/jap/98/5?ver=pdfcov
Published by the AIP Publishing

Defect dynamics in annealed ZnO by positron annihilation spectroscopy

Sreetama Dutta, Mahuya Chakrabarti,[a] S. Chattopadhyay, and Debnarayan Jana[b]
Department of Physics, University of Calcutta, 92 Acharya Prafulla Chandra Road, Kolkata 700 009, India

D. Sanyal
Variable Energy Cyclotron Centre, 1/AF, Bidhannagar, Kolkata 700 064, India

A. Sarkar
Department of Physics, Bangabasi Morning College, 19 Rajkumar Chakraborty Sarani, Kolkata 700 009, India

(Received 15 December 2004; accepted 25 July 2005; published online 13 September 2005)

As-supplied polycrystalline ZnO samples (purity 99.9% from Sigma-Aldrich, Germany) have been annealed at different temperatures and subsequently characterized by positron annihilation spectroscopy, x-ray-diffraction (XRD) analysis, thermogravimetric analysis (TGA), and resistivity measurements. Positron annihilation lifetime analysis and coincidence Doppler-broadened electron-positron annihilation γ-radiation (CDBEPAR) line-shape measurements have been employed at a time to identify the nature of defects in differently annealed ZnO materials. Annealing up to 300 °C, an increase of defect lifetime (τ_2) as well as shape parameter (S parameter) has been observed. Further annealing causes a large decrease of τ_2 and S parameter. TGA study shows considerable mass loss from ZnO as the annealing temperature is increased above 300 °C. This is possibly due to oxygen evaporation from the sample. The c-axis lattice parameter, extracted from the XRD spectra, shows an increase due to annealing above 600 °C, which is a signature of the presence of a huge number of oxygen vacancies. Resistivity variations of the annealed samples are also consistent with the TG and XRD analyses. The ratio curve analysis of the CDBEPAR spectra successfully probes the change in zinc-related vacancy defects in annealed ZnO. © *2005 American Institute of Physics*. [DOI: 10.1063/1.2035308]

I. INTRODUCTION

Investigation on ZnO is going on for decades, however, its recent surge is a matter of fact. This wide band-gap semiconducting compound has immense potential for use in next generation electro-optic devices such as ultraviolet (UV) light-emitting diodes (LEDs), blue luminescent devices, UV lasers, gas sensors,[1–3] etc. The most discussed issue related to ZnO is defects, either native or artificially incorporated.[4,5] It is well known that defects in such materials affect strongly the structural, electrical, and optical properties. A proper understanding on the nature of defects in ZnO is essential for a better tuning of material properties. Recent interest has been focused on identifying various native defects (vacancies and interstitials at O or Zn sites) and their role in heat-treated,[6–8] ion-irradiated,[9,10] or nanosized ZnO.[11] An interesting correlation of oxygen vacancy concentration and green luminescence from ZnO has also been observed.[12] In the present study, an as-supplied ZnO material has been investigated from positron annihilation spectroscopy (PAS), x-ray diffraction (XRD), thermogravimetric analysis (TGA), and resistivity measurements. The particular importance of positron annihilation spectroscopy for identification of vacancy-type defects in a solid is well known.[13,14] Fortunately, vacancy defects at zinc and oxygen sites are most abundant in the ZnO (Ref. 15) system. The evolution of such defects with increasing annealing temperature is being presented in greater detail. This paper employs the ratio curve analysis to understand the defect dynamics in ZnO due to annealing.

Positron annihilation lifetime (PAL) spectroscopy deals with the measurement of the lifetime of positrons (~100–400 ps) in a solid.[16] Positrons injected from a radioactive source (here ^{22}Na) get thermalized within 1–10 ps inside a solid and annihilate with an electron of that material. It is well known that positrons preferentially populate (and annihilate) in the regions where electron density, compared to the bulk of the material, is lower (e.g., vacancy-type defects, vacancy clusters, and microvoids). The lifetime of positrons trapped in defects is comparatively longer with respect to those that annihilate at defect-free regions. An analysis of the PAL spectrum, thus, throws light on the nature and abundance of defects in the material. The other PAS technique, Doppler broadening of the positron annihilation radiation line-shape measurement, is useful to study the momentum distribution of electrons in a material.[17,18] Depending on the electron momentum (p), the 511-keV γ rays (electron-positron annihilated) are Doppler shifted by an amount $\pm\Delta E = p_L c/2$ in the laboratory frame where p_L is the component of the electron momentum (p) along the direction of measurement. Using high-resolution high-purity germanium (HPGe) detectors one can measure the spectrum of Doppler-shift 511-keV γ rays. The wing region of the 511-keV spectra (higher value of p_L) carries the information about the annihilation of positrons with the core electrons. The mo-

[a]Present address: Variable Energy Cyclotron Centre, 1/AF, Bidhannagar, Kolkata 700 064, India
[b]Author to whom correspondence should be addressed; electronic mail: d.jana@cucc.ernet.in

menta of the core electrons are element specific[19] and hence the atoms surrounding a defect can be probed by proper analysis of the measured spectra.

II. EXPERIMENT AND DATA ANALYSIS

As-supplied polycrystalline ZnO powder has been palletized and annealed at 200, 300, 400, 600, 800, and 1000 °C for 18 h followed by slow cooling (30 °C/h) in air. The XRD data has been collected in a Philips PW 1710 automatic diffractometer with Cu $K\alpha$ radiation. The average grain size of the powdered samples has been determined by Scherrer formula.[20] The TGA of an unannealed ZnO sample has been performed in a Mettler Toledo-TGA/SDTA 851^e instrument from room temperature to 800 °C. Room-temperature resistivity measurements have been carried out by four-probe technique using a Keithley 2182 nanovoltmeter and 2400 constant current source. Very high resistances of the unannealed 200 and 300 °C samples have been measured by a two-probe Keithley 6514 electrometer. For positron annihilation studies, a 10-μCi ^{22}Na positron source (enclosed in thin mylar foils) has been sandwiched between two identical plane-faced ZnO pellets. The PAL spectra have been measured with a fast-slow coincidence assembly[16] having a 182±1-ps time resolution. Measured spectra have been analyzed by computer program PATFIT-88 (Ref. 21) with necessary source corrections to evaluate the possible lifetime components τ_i and their corresponding intensities I_i. The two-detector[22] coincidence Doppler-broadened electron-positron annihilation γ-radiation (CDBEPAR) spectrum has been measured by a HPGe detector (efficiency of 13% and energy resolution of 1.3 keV for the 514-keV line of ^{85}Sr) and a 3×3-in.^{2} NaI (Tl) crystal coupled to a RCA 8850 photomultiplier tube placed at an angle of 180°. The use of the two detectors in coincidence helps to suppress the background in the measured Doppler-broadened spectrum and hence the contributions of higher-momentum electrons (core electrons) can be estimated.[23] In the present experiment, the peak to background (607 to 615 keV) ratio is 14 000:1. The energy per channel of the multichannel analyzer has been set to 22 eV. The CDBEPAR spectra for each sample have been analyzed by evaluating the so-called shape parameter (S parameter) and wing parameter (W parameter).[18] The S parameter, calculated as the ratio of counts in the central area of the 511-keV photopeak ($|511\ \text{keV}-E_\gamma|\leqslant 0.86$ keV) and the total area of the photo peak ($|511\ \text{keV}-E_\gamma|\leqslant 4.25$ keV), represents the fraction of positrons annihilating with the lower momentum electrons. The W parameter, calculated as the ratio of counts in the wing region of the 511-keV photopeak ($1.6\ \text{keV}\leqslant|E_\gamma-511\ \text{keV}|\leqslant 4$ keV) and the total area of the photopeak, represents the fraction of positrons annihilating with the higher-momentum electrons. The ratio curves[23–25] from each CDBEPAR spectra of the ZnO samples has been constructed by dividing the counts at the same energy with that of a standard CDBEPAR spectrum (spectrum of Al single crystal in the same setup).

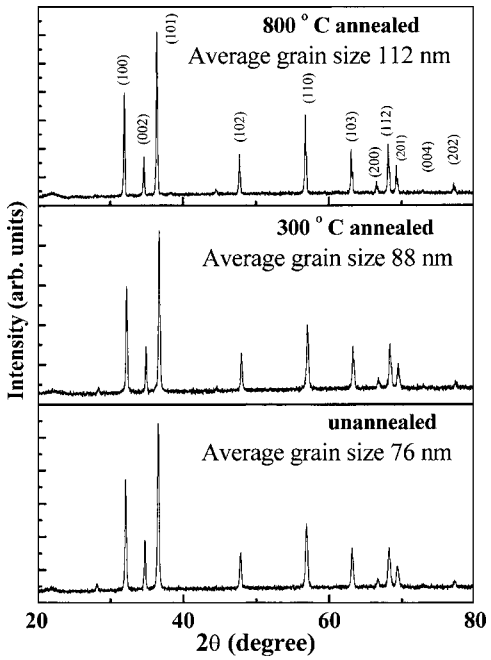

FIG. 1. X-ray-diffraction patterns for the unannealed and annealed ZnO samples.

III. RESULTS AND DISCUSSION

The XRD patterns for unannealed and annealed samples are shown in Fig. 1. The results of PAL spectra analysis for all ZnO samples have been shown in Table I and Fig. 2. All lifetime spectra are found to be best fitted with three lifetime components, yielding a very long (>1.1 ns) positron lifetime component (τ_3) with intensity ~3%. This component is due to the formation of orthopositronium and its subsequent decay as parapositronium by pick-off annihilation. In polycrystalline samples, there always exist microvoids where positronium formation is favorable.[16] The short lifetime component ($\tau_1\sim 145$ ps) is generally attributed to the free annihilation of positrons. The most important lifetime component is the intermediate one, τ_2, which arises from the annihilation of positrons at defect sites.[13] It is interesting to note that the defect lifetime in the present ZnO samples increases with annealing temperature up to 300 °C. A distinct decrease of τ_2 has been observed for annealing higher than 400 °C, which eventually saturates at 800 °C. The variation of the corresponding intensity (I_2) with the annealing temperature has been shown in the Fig. 2 as an inset. One can construct

TABLE I. Table showing the results of resistivity measurements, XRD analysis, and part of the positron lifetime analysis.

Annealing temperature (°C)	Resistivity (Ω cm)	τ_1 (ps)	I_1 (%)	τ_3 (ps)
Unannealed	8.4×10^7	147±2	38.0±0.5	1359±42
200	6.3×10^7	151±2	36.8±0.5	1339±35
300	2.7×10^7	144±2	32.5±0.5	1429±41
400	7.982×10^5	144±2	34.0±0.5	1305±33
600	5.198×10^5	155±2	46.0±0.5	1272±34
800	1.928×10^2	149±2	51.5±0.5	1205±28
1000	6.297×10^0	141±2	57.5±0.5	1441±39

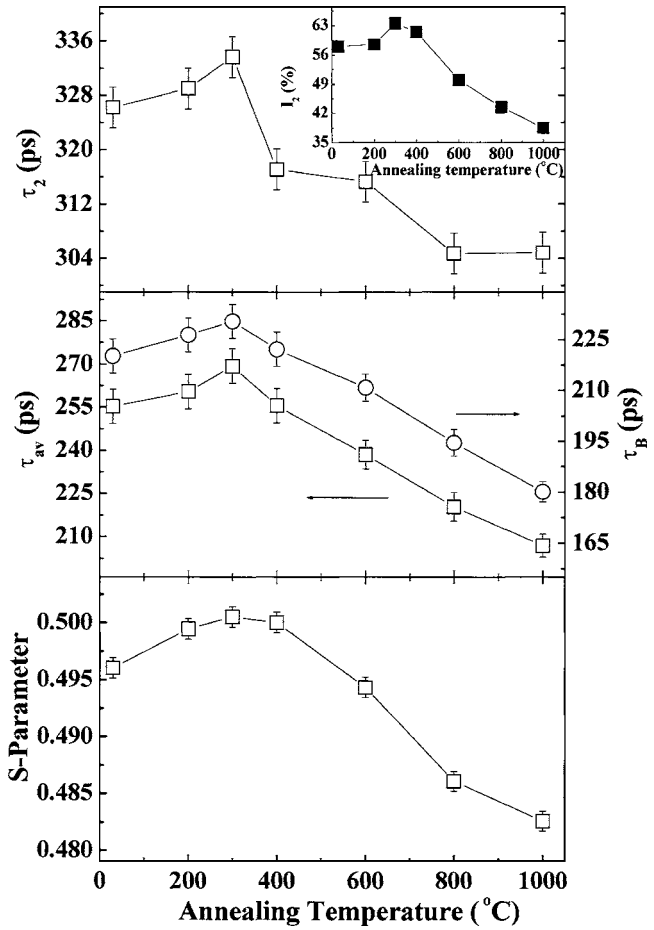

FIG. 2. Variation of τ_2 (positron lifetime at defects), average position lifetime (τ_{av}), bulk positron lifetime (τ_B), and S parameter with annealing temperature for the ZnO samples. The inset shows the variation of I_2 (intensity corresponding to τ_2) with annealing temperature. The annealing temperature of the unannealed ZnO sample has been taken as 30 °C (room temperature).

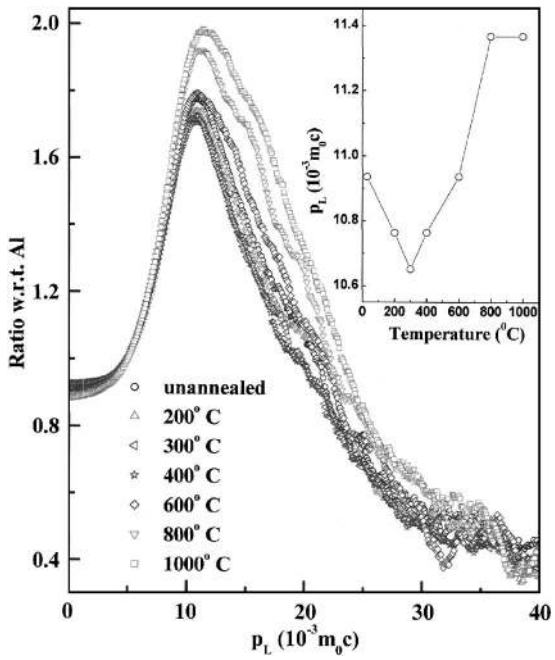

FIG. 3. Ratio curves of the experimental electron-positron momentum distributions for unannealed and annealed ZnO samples with respect to standard electron-positron momentum distribution of a defect-free Al single crystal. The inset shows the relative position of the ratio curve peaks for the ZnO samples with annealing temperature.

positron average lifetime, $\tau_{av}[=(\tau_1 I_1+\tau_2 I_2)/(I_1+I_2)]$, and positron bulk lifetime, $\tau_B[=(I_1+I_2)/(I_1/\tau_1+I_2/\tau_2)]$, from τ_1, τ_2, I_1, and I_2. An increase of τ_{av} reflects the overall enhancement of defects in the sample. Here τ_{av} and τ_B both show their respective highest values for the 300 °C annealed ZnO sample. The CDBEPAR shape parameter (S parameter) also increases slowly up to 300 °C. Such an increase is due to an enhancement of open volume defects in the system and a subsequent increase of lower-momentum electron contribution in CDBEPAR spectra. The S parameter starts to decrease from 400 °C annealing. For 1000 °C-annealed ZnO it reaches to its lowest value. A decrease of S parameter indicates increasing annihilation of positrons with higher-momentum electrons or core electrons. To identify these higher-momentum electrons, CDBEPAR spectra for the unannealed and annealed ZnO samples have been analyzed by constructing ratio curves with the CDBEPAR spectrum of the defect-free Al single crystal (Fig. 3). Figure 3 shows a peak at the momentum value $\sim 11\times10^{-3}$ m_0c for unannealed and annealed samples. The important result is that the peak heights for the 600, 800, and 1000 °C-annealed samples are quite large compared to that of the unannealed and 200, 300, and 400 °C-annealed samples. Generally, ratio curves of the oxide materials[19,25] with respect to Al or Si show a peak near 11×10^{-3} m_0c, which is the contribution of oxygen $2p$ electrons in the annihilation process. But the scenario in ZnO becomes intriguing as pure Zn may also contribute to this peak.[19,26] In fact, the peak positions in Fig. 3 shift systematically towards the higher momentum for the samples annealed above 400 °C (inset of Fig. 3). A shoulder, although not very prominent, appears near a momentum value of 17×10^{-3} m_0c for 800 and 1000 °C-annealed samples. The exact position and its relative intensity may be found after perfect deconvolution[19] of such ratio curves and has been attributed as the signature of positron annihilation with the $3s$ electrons of Zn. So, it is evident that positrons annihilate more with electrons of the Zn atoms in case of samples annealed at 600, 800, and 1000 °C than the other samples. Higher vacancy concentration in a sample leads to larger positron annihilation probability with low-momentum valence electrons. The strongly bound core electrons, closer to the nucleus, have little probability of annihilation with positrons inside a vacancy such as free space. Reduction of Zn vacancies allows more positrons to be annihilated in the defect-free regions of a ZnO crystal. Consequently, the annihilation of positrons with the core electrons of zinc and oxygen is increased. The positron annihilation with core electrons of oxygen is insignificant[27] and the Zn core electrons mainly contribute to the higher-momentum part of the CDBEPAR spectrum. To get a little more insight into the scenario, the ratio curves of the annealed samples with respect to the unannealed one has been presented in Fig. 4. A clear difference in the ratio curves between the 600, 800, and 1000 °C-annealed and 200 and 300 °C-annealed samples can be observed above the momentum value 5×10^{-3} m_0c. The appearance of the prominent dip in the momentum value

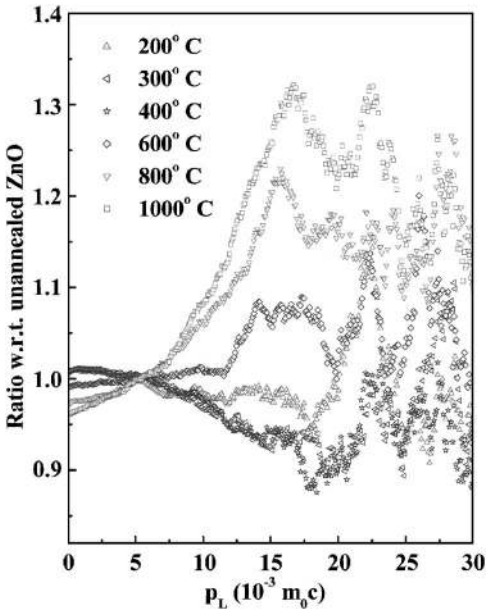

FIG. 4. Ratio curve of the experimental electron-positron momentum distributions for the annealed ZnO samples with respect to the same unannealed ZnO.

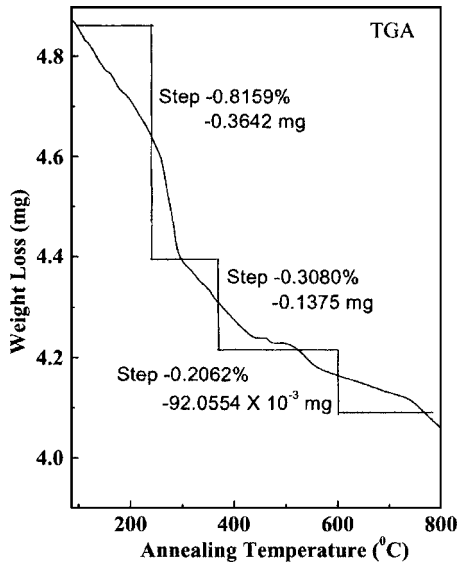

FIG. 5. TGA curve of the unannealed ZnO sample.

$\sim 17 \times 10^{-3}$ m_0c represents that in 200 and 300 °C-annealed samples positrons are less annihilating with the core electrons of the Zn ions. The presence of Zn vacancies in these samples, presumably as vacancy clusters at grain boundaries,[28] can be understood. Typical values of positron lifetimes originating from O vacancy and Zn vacancy in ZnO are, respectively, 180 and 237 ps.[4] The defect lifetime of τ_2 ~ 330 ps, as observed in our case, also supports the clustering of Zn vacancies. However, few Zn vacancies may also exist within the grains. As the annealing temperature is increased from room temperature, the intragrain Zn vacancies gradually move to their more favored grain-boundary regions where the annihilation probability of positrons is very high. This fact is reflected from the increase of τ_2, τ_{av}, and S parameter with annealing temperatures up to 300 °C. Such an increase of the positron annihilation parameters is typical for polycrystalline[28] or irradiated ZnO (Refs. 9 and 10) samples. In fact, we have recently observed[29] similar results in nanocrystalline ZnO. In single-crystalline ZnO, Zn vacancies exist[4] but their concentration is low and uniform. Hence, the agglomeration of defects in some preferred regions (for heating up to 300 °C) does not take place and the subsequent increase of τ_2, τ_{av}, and S parameter has not been observed.[9] Above some annealing temperature, oxygen vacancy formation predominates in ZnO material (detailed in the next paragraph) and Zn interstitials are also generated. These Zn interstitials become mobile at higher temperatures and recombine with Zn vacancies and a decrease in τ_2, τ_{av}, and S parameter is observed. The observed small grain growth in the annealed samples (Fig. 1) is due to the annihilation of Zn vacancy defects from the grain boundaries.

To confirm the oxygen vacancy formation in ZnO due to annealing, TGA and XRD analyses have been performed. The mass loss with increasing temperature as seen in the TGA curve of Fig. 5 is due to oxygen evaporation[8] from the sample. Maximum loss occurred at the temperature range of 250–370 °C. The effect of annealing on the *c*-axis lattice parameter calculated from (002) peaks of each x-ray diffractograms has been shown in Fig. 6. The presence of considerable oxygen vacancies expands the ZnO lattice[30] as is seen from the variation of the *c*-axis length. Results of resistivity measurement (Table I) also show a huge reduction of resistivity for the samples annealed at temperatures higher than 300 °C. This is also consistent with the increase of native oxygen vacancies in the system.

At this juncture, we should recall that oxygen vacancies in ZnO (Refs. 4, 8, and 13) mostly bear positive charges and cannot trap positrons. This is in general true for positively charged anion vacancies in II-VI semiconductors. However, low-temperature positron lifetime results on ZnO cannot completely rule out a weak but finite positron trapping at oxygen vacancies at room temperature.[4] To identify the different positron trapping sites, if any, we have also plotted the

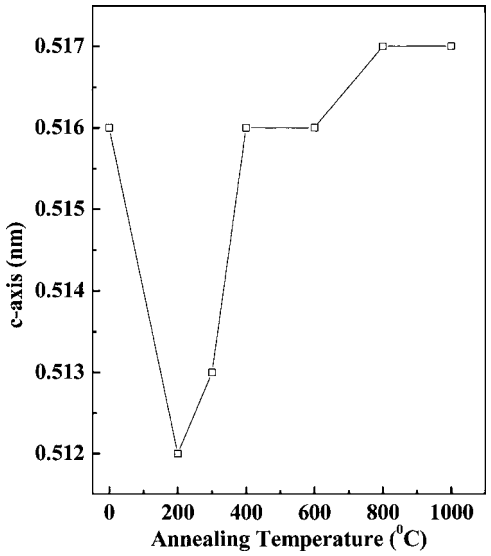

FIG. 6. Variation of *c*-axis lattice parameter of ZnO with annealing temperature.

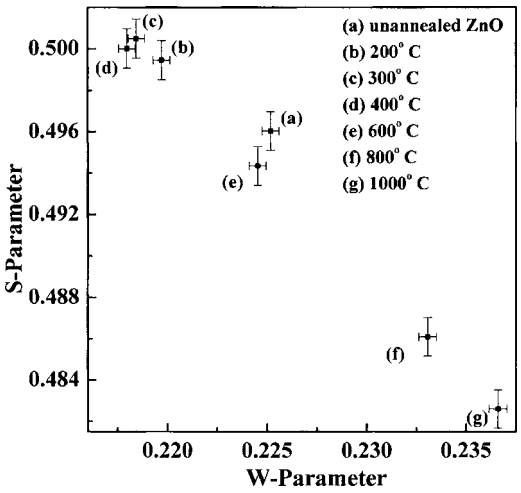

FIG. 7. Variation of *S* parameter with *W* parameter for unannealed and annealed ZnO samples.

S parameter versus *W*-parameter graph (Fig. 7). To the limit of our experimental accuracy, the variation can be understood as a linear one, which denotes only one major positron-trapping site. However, with improved accuracy and higher statistics, the possibility of another defect site cannot completely be excluded. Although XRD, TGA, and resistivity measurements conclusively reveal the presence of oxygen vacancies in ZnO (above 300 °C annealing), room-temperature positron annihilation studies fail to reconfirm it at this stage.

IV. CONCLUSION

The present study reports the dynamics of defect formation and annihilation in polycrystalline ZnO with annealing temperatures up to 1000 °C. In polycrystalline ZnO, Zn vacancy defects predominate up to an annealing temperature of 300 °C. With further annealing more and more oxygen vacancy is generated as evident from the variation of resistivity and *c*-axis lattice parameter with annealing temperature. Ratio curve analysis of the CDBEPAR spectra can identify the enhancement/lowering of positron trapping at Zn vacancies with annealing. Such analysis does not bear any information regarding the possible positron trapping at oxygen vacancies. The initial rise of positron lifetime and CDBEPAR parameters with increasing annealing temperature is related to the grain-boundary effect of polycrystalline ZnO. It is to be noted that a similar feature does not arise in single crystals.

ACKNOWLEDGMENTS

The authors acknowledge the help from Professor A. Ghosh, Department of Chemistry, University of Calcutta, for thermogravimetric analysis. Two of the authors (S.C. and M.C.) gratefully acknowledge CSIR, Government of India for providing financial assistance. We are also grateful to FIST-DST for providing financial assistance.

[1] D. C. Look, J. W. Hemsky, and J. R. Sizelove, Phys. Rev. Lett. **82**, 2552 (1999).
[2] D. C. Reynolds, D. C. Look, and B. Jogai, Solid State Commun. **99**, 873 (1996).
[3] I. Stambolova, K. Konstantinov, S. Vassilev, P. Peshev, and Ts. Tsacheva, Mater. Chem. Phys. **63**, 104 (2000).
[4] F. Tuomisto, V. Ranki, K. Saarinen, and D. C. Look, Phys. Rev. Lett. **91**, 205502 (2003).
[5] K.-K. Kim, H.-S. Kim, D.-K. Hwang, I.-H. Lim, and S.-J. Park, Appl. Phys. Lett. **83**, 63 (2003).
[6] N. R. Aghamalyan, I. A. Gambaryan, E. Kh. Goulanian, R. K. Hovsepyan, R. B. Kostanyan, S. I. Petrosyan, E. S. Vardanyan, and A. F. Zerrouk, Semicond. Sci. Technol. **18**, 525 (2003).
[7] T.-B. Hur, G. S. Jeen, Y.-H. Hwang, and H.-K. Kim, J. Appl. Phys. **94**, 5787 (2003).
[8] Z. Q. Chen, S. Yamamoto, M. Maekawa, A. Kawasuso, X. L. Yuan, and T. Sekiguchi, J. Appl. Phys. **94**, 4807 (2003).
[9] S. Brunner, W. Puff, P. Mascher, and A. G. Balogh, Mater. Res. Soc. Symp. Proc. **540**, 207 (1999).
[10] Z. Q. Chen, M. Maekawa, T. Sekiguchi, R. Suzuki, and A. Kawasuso, Mater. Sci. Forum **445–446**, 57 (2004).
[11] R. Radoi, P. Fernández, J. Piqueras, M. S. Wiggins, and J. Solis, Nanotechnology **14**, 794 (2003).
[12] K. Vanheusden, C. H. Seager, W. L. Warren, D. R. Tallant, and J. A. Voigt, Appl. Phys. Lett. **68**, 403 (1996).
[13] R. Krause-Rehberg and H. S. Leipner, *Positron Annihilation in Semiconductors* (Springer, Berlin, 1999), Chap. 3, p. 61.
[14] M. Chakrabarti, S. Dutta, S. Chattopadhayay, A. Sarkar, D. Sanyal, and A. Chakraborti, Nanotechnology **15**, 1792 (2004).
[15] A. F. Kohan, G. Ceder, D. Morgan, and C. G. Van de Walle, Phys. Rev. B **61**, 15019 (2000).
[16] D. Sanyal, D. Banerjee, and U. De, Phys. Rev. B **58**, 15226 (1998).
[17] U. De, D. Sanyal, S. Chaudhuri, P. M. G. Nambissan, Th. Wolf, and H. Wühl, Phys. Rev. B **62**, 14519 (2000).
[18] M. Chakrabarti, A. Sarkar, S. Chattapadhayay, D. Sanyal, A. K. Pradhan, R. Bhattacharya, and D. Banerjee, Solid State Commun. **128**, 321 (2003).
[19] U. Myler and P. J. Simpson, Phys. Rev. B **56**, 14303 (1997).
[20] B. E. Waren, *X-ray Diffraction* (Addison-Wesley, Reading, MA, 1969), p. 26419.
[21] P. Kirkegaard, N. J. Pedersen, and M. Eldrup, Riso National Lab, Report No. Riso-M-2740, 1989.
[22] K. G. Lynn and A. N. Goland, Solid State Commun. **18**, 1549 (1976).
[23] R. S. Brusa, W. Deng, G. P. Karwasz, and A. Zecca, Nucl. Instrum. Methods Phys. Res. B **194**, 519 (2002).
[24] P. Asoka-Kumar, M. Alatalo, V. J. Ghosh, A. C. Kruseman, B. Nielsen, and K. G. Lynn, Phys. Rev. Lett. **77**, 2097 (1996).
[25] M. Chakrabarti, A. Sarkar, D. Sanyal, G. P. Karwasz, and A. Zecca, Phys. Lett. A **321**, 376 (2004).
[26] V. J. Ghosh, M. Alatalo, P. Asoka-Kumar, B. Nielsen, K. G. Lynn, A. C. Kruseman, and P. E. Mijnarends, Phys. Rev. B **61**, 10092 (2000).
[27] F. Plazaola, A. P. Seitsönen, and M. J. Puska, J. Phys.: Condens. Matter **6**, 8809 (1994).
[28] T. K. Gupta, W. D. Straub, M. S. Ramanachalam, J. P. Schaffer, and A. Rohatgi, J. Appl. Phys. **66**, 6132 (1989).
[29] A. Sarkar, S. Chattopadhayay, S. Dutta, S. Bid, S. K. Pradhan, A. Banerjee, and D. Jana (unpublished).
[30] H. Kim, A. Piqué, J. S. Horwitz, H. Murata, Z. H. Kafafi, C. M. Gilmore, and D. B. Chrisey, Thin Solid Films **377–378**, 798 (2000).